

# The three-dimensional porous mesh structure of Cu-based metal-organic-framework - aramid cellulose separator enhances the electrochemical performance of lithium metal anode batteries

Manshu Zhang <sup>a,1</sup>, Liming Wu <sup>a,1</sup>, Tao Yang <sup>b</sup>, Bing Zhu <sup>a</sup>, Yangai Liu <sup>a,\*</sup>

<sup>a</sup> Beijing Key Laboratory of Materials Utilization of Nonmetallic Minerals and Solid Wastes, National Laboratory of Mineral Materials, School of Material Science and Technology, China University of Geosciences, Beijing 100083, China

<sup>b</sup> College of Materials & Environmental Engineering, Hangzhou Dianzi University, Hangzhou 310036, China

## ARTICLE INFO

### Keywords:

Lithium metal battery  
Lithium dendrites  
CuMOF-ANFs separator

## ABSTRACT

Lithium metal, due to its advantages of high theoretical capacity, low density and low electrochemical reaction potential, is used as a negative electrode material for batteries and brings great potential for the next generation of energy storage systems. However, the production of lithium metal dendrites makes the battery life low and poor safety, so lithium dendrites have been the biggest problem of lithium metal batteries. This study shows that the larger specific surface area and more pore structure of Cu-based metal-organic-framework - aramid cellulose (CuMOF-ANFs) composite separator can help to inhibit the formation of lithium dendrites. After 110 cycles at 1 mA/cm<sup>2</sup>, the discharge capacity retention of the Li-Cu battery using the CuMOF-ANFs separator is about 96 %. Li-Li batteries can continue to maintain low hysteresis for 2000 h at the same current density. The results show that CuMOF-ANFs composite membrane can inhibit the generation of lithium dendrites and improve the cycle stability and cycle life of the battery. The three-dimensional (3D) porous mesh structure of CuMOF-ANFs separator provides a new perspective for the practical application of lithium metal battery.

## 1. Introduction

Certainly, here is a possible introduction for your topic:Lithium-metal batteries are promising candidates for high-energy-density rechargeable batteries due to their low electrode potentials and high theoretical capacities [1,2]. However, during the cycle, dendrites forming on the lithium metal anode can cause short circuit, which can affect the safety and life of the battery [3–9]. Therefore, researchers are indeed focusing on various aspects such as negative electrode structure [10], electrolyte additives [11,12], SEI film construction [13,14], and collector modification [15] to inhibit the formation of lithium dendrites. However, using a separator with high mechanical strength and chemical stability is another promising approach to prevent dendrites from infiltrating the cathode. By incorporating a separator with high mechanical strength, it can act as a physical barrier to impede the growth of dendrites. This barrier can withstand the mechanical stress exerted by the dendrites during battery operation, preventing them from reaching the cathode and causing short circuits or other safety issues. Moreover,

chemical stability of the separator is equally important as it ensures that the separator remains intact and does not react or degrade in the presence of the electrolyte or other battery components. A chemically stable separator helps to prevent the formation of reactive species that can further promote dendrite growth. Researchers are actively exploring different materials and designs for separators to enhance their mechanical strength and chemical stability. These efforts aim to create separators that can effectively block dendrite formation, thereby improving the safety and performance of lithium-ion batteries. While there are several research directions to address the issue of dendrite formation, using a separator with high mechanical strength and chemical stability is an important approach to prevent dendrites from infiltrating the cathode and ensure safe operation of lithium metal batteries.

Several types of separators currently used in research include nanoporous polymer separators [16], ceramic composite separators [17], nanofiber separators [18–20], and metal-organic skeleton (MOF) separators [21–24]. While these separators have shown some ability to inhibit the growth of lithium dendrites, they still have some drawbacks,

\* Corresponding author.

E-mail address: liuyang@cugb.edu.cn (Y. Liu).

<sup>1</sup> These authors contributed equally.

which is why researchers are continuing their work. Nanoporous polymer separators have high electrical conductivity and excellent mechanical properties, which can effectively inhibit dendrite growth and reduce their size. However, these separators have low ion permeability and pose a fire risk. Ceramic composite separators exhibit high temperature and chemical stability, preventing dendrite growth and improving battery life. Unfortunately, they are costly to prepare and may decrease the energy density of the battery. Nanofiber separators possess excellent ion transport performance and mechanical strength while also preventing dendrite growth. However, the complex preparation method and the risk of flammability and unstable explosion are concerns. MOF separators belong to a class of porous materials with high surface area and excellent ion permeability, enhancing battery energy density and cycle life. However, the stability and cost of preparing MOF separators still require further optimization.

For many years, more researchers have been dedicated to using MOF separators to suppress the growth of lithium dendrites [25–29]. For example, Fu, Shiyang et al. studied a cake shaped TiO<sub>2</sub> coating with a metal organic framework derivative on the separator [29]. Although various MOF separators studied can effectively improve the dendrite suppression effect of lithium metal batteries and also have a certain effect on improving the cycling stability of batteries, further exploration is needed to improve the cycling life of lithium metal batteries and reduce material usage costs. Therefore, in this work, we studied the application of CuMOF - aramid cellulose composite separator in lithium metal batteries. The CuMOF phase provides mechanical strength and chemical stability, while the aramid cellulose enhances ion selectivity and can effectively reduce the occurrence of side reactions in electrochemical reactions, thereby improving the electrochemical performance of the battery. This work aims to improve the safety and performance of lithium metal batteries by developing effective separators based on CuMOF-ANFs composites.

## 2. Experimental

### 2.1. Materials

Copper nitrate trihydrate granules, 1, 3, 5-benzoic acid granules and anhydrous ethanol solution purchased from Aladdin. A coin-type cell (CR2032), PP separator, and Cu foil were chosen as the parts for constructing the batteries, and they were all from Shenzhen KejingZhida Technology Co., Ltd. The mixed 80% microporous membrane was purchased from Shanghai Compact Film Separation Technology Co., Ltd. Li foil was prepared from Beijing Vinbeido Technology Co., Ltd., and the electrolyte was 1 mol/L LiTFSI in DOL/EMC ( $v/v = 1:1$ ) with 0.1 mol/L LiNO<sub>3</sub> [30].

### 2.2. Preparation of CuMOF-ANF separator

3.6 mmol copper nitrate trihydrate was mixed with 12 ml distilled water to form solution A, and then 0.42mmol 1, 3, 5-benzoic acid was mixed with 12 ml anhydrous ethanol solution to form solution B. Then, the solutions A and B were mixed with 1 ml aramid cellulose at room temperature for 30 min, and then poured into the inner lining of a clean reactor. After heating in a vacuum drying oven at 120 °C for 12 h, the solution was obtained and filtered on a vacuum pumping filter. The obtained solids were dried in a vacuum drying oven for 24 h under the condition of 60 °C and ground in a mortar for 15 min. Then, the blue CuMOF-ANFs powder was prepared. The preparation of the CuMOF-ANFs composite slurry requires mixing the CuMOF-ANFs powder with the binder at a ratio of 8:1 and grinding it uniformly with N, n-dimethylamide for 20 min to ensure that the slurry is not obviously granular. The PP separator was uniformly coated with CuMOF-ANFs slurry, and the separator was put into a vacuum drying oven and dried at 60 °C for 24 h. After drying, the composite separator was cut into circular slices with a diameter of 15 mm, and finally the CuMOF-ANFs separator was

obtained.

## 2.3. Characterization

### 2.3.1. X-ray diffraction

CuMOF-ANFs powder was dispersed in ethanol and applied to monocrystalline silicon zero-background scaffolds. X-ray diffraction experiments were then performed with the Rigaku SmartLab SE instrument equipped with Cu-Kα radiation and the Lynxeye detector at angles ranging from 5° to 80°.

### 2.3.2. Morphological characterization

The morphology of the CuMOF-ANFs separator and the recycled lithium sheet was observed using a Field Emission Gun Scanning Electron Microscope y (FE-SEM, S-4800, Japan). Before the observation, a thin layer of gold was sprayed on the separator to prevent electron charging. However, no gold spraying was required on the lithium sheet. The acceleration voltages used for the observations were 2 kV and 10 kV [31].

### 2.3.3. X-ray photoelectron spectroscopy

The X-ray photoelectron spectroscopy (XPS) analysis was conducted using a Micrometrics VSCALABXi spectrometer equipped with a monochromatic Al Kα X-ray source. The X-ray energy was set at 1486.6 eV, which corresponds to the Al Ka X-ray emission line. The instrument was operated at a power of 225 W. To ensure accurate measurements, the vacuum conditions in the spectrometer chamber were maintained at  $1 \times 10^{-9}$  mbar. The separator with CuMOF-ANFs coating was tested. This low-pressure environment helps minimize interference from air molecules and ensures reliable data acquisition. During the XPS analysis, the binding energy was set to 284.2 eV [32].

### 2.3.4. Nitrogen adsorption

Nitrogen adsorption analysis was performed using a Autosorb-iQ surface area analyzer, at –194 °C, to look at the separator's mesoporous, the specific surface area and pore size were calculated by Bruner-Emmet-Teller (BET) and Barrett-Joyner-Halenda (BJH) methods, respectively.

### 2.3.5. FT-IR spectroscopy

In order to verify the presence of functional groups in CuMOF and CuMOF-ANFs composite separator, Fourier transform infrared (FT-IR, Nicolet™ iSTM 5) spectra were recorded using the Bruker TENSOR II Fourier Transform Infrared Spectrometer. The spectra were obtained in the range of 4000–400 cm<sup>-1</sup> with a spectral resolution of 4 cm<sup>-1</sup>. In order to improve the signal-to-noise ratio, each spectrum was averaged over 32 scans [31].

### 2.3.6. Contact angle analysis

Assessing the wetting of the diaphragm surface to the electrolyte requires the use of a contact Angle/interfacial tensiometer (JC2000D). The whole process needs to be operated in the glove box, the separator with a diameter of 15 mm is completely immersed in the electrolyte, and the liquid absorption rate and electrolyte retention rate of the membrane are measured.

### 2.3.7. Thermogravimetric analysis

The thermogravimetric test (TGA) of the CuMOF-ANFs separator was performed with a thermal analyzer (Hitachi TG/DTA7200). It is important to dry the separator completely before testing. The temperature rise was measured from 30 °C to 600 °C at a rate of 10 °C/min under nitrogen atmosphere [31].

### 2.3.8. Electrochemical characterization

Electrochemical impedance spectroscopy (EIS) measurements of the battery after different cycles were performed on the PARSTAT-2273

electrochemical workstation with an amplitude of 10 mV in the frequency range of 100 kHz to 100 mHz.

EIS is commonly used to evaluate the diffusion coefficient of lithium ions in battery materials. The low-frequency Warburg impedance observed in the EIS plot is directly related to the diffusion process of lithium ions in the electrode material. The high-frequency intercept on the real axis ( $Z_{\text{real}}$ ) represents the resistance of the electrolyte. The semicircle in the high-frequency range indicates charge transfer resistance, while the low-frequency slashes are attributed to the diffusion of lithium ions in the electrode material. The diffusion coefficient of lithium ions can be calculated using the following formula [33]:

$$D = \frac{R^2 T^2}{2A^2 n^4 F^4 C^2 \sigma^2}$$

Where R is the gas constant, T is the absolute temperature, A is the surface area of the cathode, n is the number of electrons per molecule in the oxidation process, F is the Faraday constant (96,486 C/mol), C is the concentration of lithium ions, and  $\sigma$  is the Warburg factor. The relationship is as follows:

$$Z_{\text{real}} = R_e + R_{\text{ct}} + \sigma \omega^{-1/2}$$

Where  $R_e$  is the resistance between the electrolyte and electrode, and  $R_{\text{ct}}$  is the charge transfer resistance,  $\omega$  is angle frequency [34].

The electrochemical stability of the diaphragm was evaluated by cyclic voltammetry (CV) in the potential range of 0.01 ~ 3 V at different potential sweep rates of 1 mV s<sup>-1</sup>. LAND equipment was used to test Cu-Li half cells and Li-Li symmetric cells with and without CuMOF-ANFs separators, respectively, to observe the electrochemical performance of the battery after cyclic reaction, such as rate performance, Coulomb efficiency, etc. Lithium iron phosphate powder, conductive carbon black and PVDF (mass ratio 8:1:1) were mixed in NMP, thoroughly ground to make a uniform cathode slurry, evenly coated on aluminum foil, and dried in a vacuum drying oven at 60 °C for 24 h. Finally, the completely dry electrode is assembled with the lithium electrode and diaphragm using a tablet press to form a full battery.

### 3. Results and discussion

**Fig. 1a** shows the XRD pattern of CuMOF-ANFs powder, indicating a well-defined crystal structure. The pattern displays strong diffraction peaks that align closely with the standard cards. **Fig. 1b**, the CuMOF-ANFs separator XPS diagram reveals two prominent peaks at 934.5 eV and 954.5 eV, corresponding to the Cu 2p<sub>3/2</sub> and Cu 2p<sub>1/2</sub> states of Cu in CuMOF, respectively. These XPS results confirm the presence of Cu. The

successful coating of CuMOF-ANFs on the polypropylene separator is evident. The micromorphology of the prepared CuMOF-ANFs powder material was observed (**Fig. 1c, d**), and it was found that the CuMOF-ANFs powder material was in regular octahedral shape with small spherical particles attached to the surface. The cross-section of the separator is further observed and the thickness of the separator is measured. As shown in figure S1, the thickness of the ordinary PP separator is 5.9 mm, while the thickness of the CuMOF-ANFs separator is 6.3 mm. It shows that copper powder has obvious morphology and clear geometric characteristics. The regular octahedral shape of the CuMOF-ANFs powder indicates that it has a crystal structure in which the atoms are arranged in a symmetrical manner. This type of shape provides a larger surface area for chemical reactions and enhances mechanical properties. **Table 1** presents the elemental composition of CuMOF-ANFs, demonstrating that the separator mainly consists of Cu, C, and O elements. The contact angles of the CuMOF-ANFs separator and PP separator on the electrolyte droplets were measured respectively, and the wettability of the electrolyte coated with the CuMOF-ANFs separator was compared on a macroscopic scale (**Fig. 1e, f**). The contact angles of CuMOF-ANFs separator and PP separator were 13° and 35°, respectively, indicating that the separator coated with CuMOF-ANFs had more polar functional groups and better compatibility between electrolyte and CuMOF-ANFs separator. Moreover, the CuMOF-ANFs separator can completely absorb the electrolyte almost instantaneously. Unfortunately, the absorption time of ordinary PP separator is longer, which also indicates the strong affinity between the CuMOF-ANFs separator and the electrolyte, which can improve the absorption capacity of the electrolyte, promote the transmission of Li+, and reduce the interface impedance [49]. Therefore, the abundant polar functional groups interact with lithium through electrostatic interaction, driving the uniform deposition of lithium [35,36].

Thermogravimetric analysis (**Fig. 2a**) revealed the thermal stability of the CuMOF-ANFs separator. The first weight loss at around 100 °C is

**Table 1**  
the CuMOF-ANFs elements of the separator.

Element	Weight percent (%)	Atomic percentage
Cu	31.26	9.39
C	21.61	34.35
O	47.13	56.26

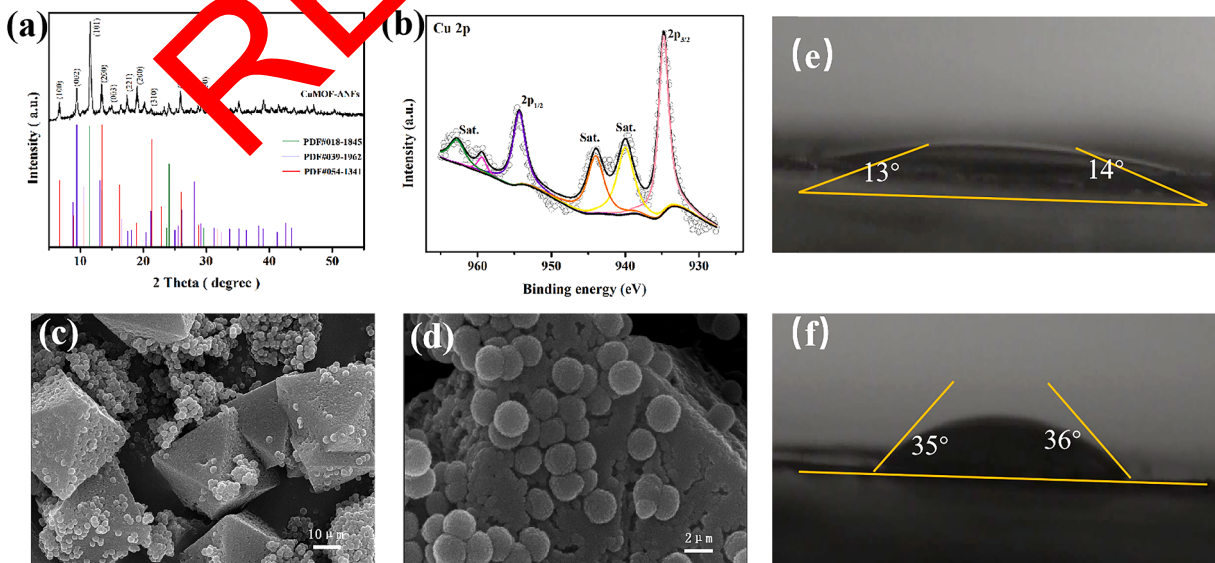


**Fig. 1.** (a) XRD of CuMOF-ANFs (b) XPS spectra of CuMOF-ANFs (c,d) SEM images of CuMOF-ANFs (e,f) Contact angle test of CuMOF-ANFs separator and pp separator respectively.

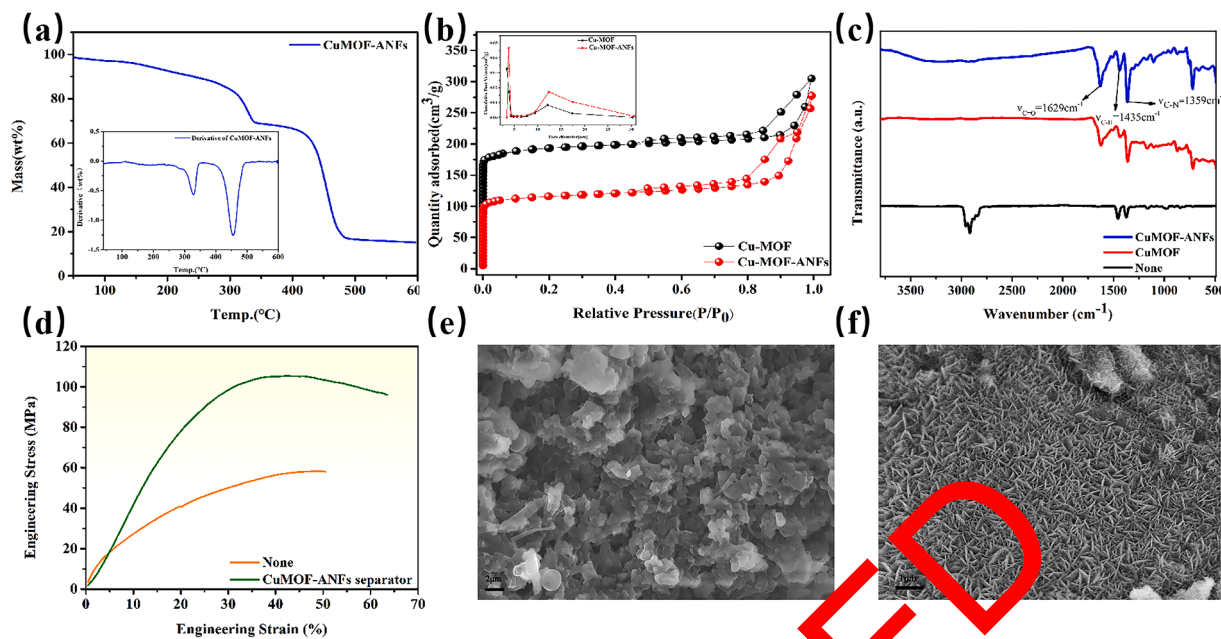


**Fig. 2.** (a) TGA curves of CuMOF-ANFs separator (b) Pore size distribution from N<sub>2</sub> sorption and relative pressure curve of adsorption (c) FTIR spectra (d) Stress-strain curves (e) SEM images of lithium sheet after 500 cycles of battery with CuMOF-ANFs separator (f) SEM images of lithium sheet after 500 cycles of battery with PP separator.

attributed to the evaporation of residual water within the CuMOF-ANFs composite, which accounts for a small percentage of the total mass loss. The second weight loss, occurring between 340 °C and 470 °C, is attributed to the removal of molecular fragments such as O—H and C—OH groups. Finally, the weight loss at 470–600 °C is due to the decomposition of the cellulose skeleton within the composite. These results indicate that the incorporation of aramid cellulose contributes to the improved thermal stability of the composite membrane, preventing its degradation to a certain extent [31]. Fig. 2b and S3 depict the N<sub>2</sub> adsorption removal curve and pore size distribution of the CuMOF-ANFs separator. According to BJH analysis, the average pore size of the separator is determined to be 24.855 nm, indicating a mesoporous structure. Following the aperture classification subdivision and supplement by IUPAC in 2015, the separator is classified as a nanopore. The specific surface area of the CuMOF-ANFs composite is measured to be 766.624 m<sup>2</sup>/g, surpassing that of Cu-MOF (434.44 m<sup>2</sup>/g). This indicates that the incorporation of aramid cellulose not only creates new voids within the material but also increases its porosity. The growth and unique structure of the composite results in a more uniform distribution of aramid on the CuMOF material. The larger specific surface area and higher pore structure enhance the surface adsorption performance of the catalyst and generate more active sites, thereby facilitating the degradation reaction [37]. Fig. 2c presents the infrared spectrum of the CuMOF-ANFs separator. The spectrum reveals that the N—H typical band of ANFs coincides with the expansion band of —OH stretching vibration, ranging from 3650 to 3000 cm<sup>-1</sup>. Additionally, the peaks at 1653, 1542, and 1514 cm<sup>-1</sup> correspond to C=O stretching in amide, N—H bending in phenyl, and C—N stretching vibration, respectively. The characteristic peaks of the CuMOF crystal structure, such as Cu-O and Cu-N peaks at 600–700 cm<sup>-1</sup>, are also observed. Notably, the intensity of the CuMOF-ANFs peak appears to have been enhanced. This enhancement can be attributed to the presence of numerous functional groups on the separator's surface, which interact with lithium ions and consequently increase the separator's adsorption capacity for lithium ions [18]. This heightened adsorption capacity ultimately contributes to the improvement of the electrochemical performance and cycle life of lithium metal anode batteries. In addition, the battery separator must maintain its toughness and strength during long-term use, which is used

to ensure the integrity of the diaphragm structure during the battery cycle and reduce safety accidents caused by physical damage or chemical reaction. Therefore, the mechanical properties of the separator are also very important, and the mechanical properties of the CuMOF-ANFs separator are tested (Fig. 2d). It can be seen from the stress-strain curve that the CuMOF-ANFs separator has better mechanical properties than the ordinary PP separator. The test results show that because aramid cellulose has very high strength, high tensile properties and high toughness, the CuMOF-ANFs separator can better withstand the tensile stress, reduce the risk of fracture and rupture, and improve the durability of the separator. To further verify the performance of CuMOF-ANFs separators, Differential Scanning Calorimetry (DSC) and Thermomechanical Analysis Method (TMA) testing are excellent methods. From the S3 (a) figure, it can be seen that the thermal closure temperature of CuMOF-ANFs separator and commercially available PP separator is not significantly different, indicating that the prepared CuMOF-ANFs separator has a certain degree of thermal stability. At the same time, it also indicates that when the operating temperature of lithium metal batteries is too high, the CuMOF-ANFs separator will automatically close the micropores that originally allowed lithium ions to freely pass through, preventing the danger of short circuits or even explosions caused by lithium ions in positive, high, and high currents, which can serve as a special protection mechanism. From the TMA test chart of S3 (b), it can be seen that with the increase of temperature, the reduction degree of CuMOF-ANFs separator is lower than that of PP separator, indicating that CuMOF-ANFs separator has better thermal stability. These advantages will improve the overall mechanical performance of the separator, so that this 3D porous mesh structure of the separator can be applied to various fields. After 500 cycles, the battery was disassembled, and the morphology of the lithium sheets (Fig. 2f) clearly showed the formation of numerous dendritic dendrites on their surface. However, as depicted in Fig. 2e, the presence of lithium dendrites on the surface of the disassembled lithium sheets from the battery with a CuMOF-ANFs separator was barely discernible. This indicates that the CuMOF-ANFs separator was effective in inhibiting the formation of lithium dendrites.

The electrochemical impedance spectroscopy (EIS) of Cu-Li half cells with CuMOF ANFs separator and cells with ordinary PP separator were

performed at room temperature respectively. After analyzing the impedance diagram (Fig. 3a), it is evident that the CuMOF-ANFs separator exhibits an interface resistance of  $97 \Omega$ , whereas the common PP separator shows an interface resistance of  $123 \Omega$ . This indicates that the CuMOF-ANFs separator possesses a lower interface resistance and better interface compatibility. Further investigation reveals that the interfacial charge transfer impedance between the ANFs separator and lithium metal electrode is lower, and the interfacial compatibility is improved. This enhancement is attributed to the improved absorption performance of the ANFs separator on the electrolyte. The composite coatings of CuMOF and ANFs have a high solubility for the carbonate electrolyte, facilitating the formation of a gel layer with adhesive properties at the separator/electrode interface. Consequently, this leads to tight interface contact and efficient charge transfer. Moreover, the gel layer formed by encapsulating the liquid electrolyte reduces the occurrence of side reactions between the solvent and the lithium electrode. This reduction inside reactions leads to a decrease in the thickness of the solid electrolyte interface (SEI) film, which in turn promotes efficient charge transfer at the electrode interface of the separator. The improved interfacial compatibility between the composite separator and the electrode helps to mitigate ohmic polarization during the charge-discharge reaction [18,38]. After subjecting the Cu-Li half battery to 50 cycles at a current density of  $1 \text{ mA/cm}^2$ , the electrochemical impedance was measured for both the CuMOF-ANFs separator and the ordinary PP separator (Fig. 3b). At a frequency of 0.01 Hz, the Cu-Li half-cell with the CuMOF-ANFs separator showed an impedance of approximately  $5861 \Omega$ , whereas the normal separator exhibited an impedance of  $9318 \Omega$ . The lower impedance observed in the CuMOF-ANFs separator can be attributed to its three-dimensional porous mesh structure. Additionally, the lithium ion conduction rate for the CuMOF-ANFs separator was found to be  $4.8210^{-17} \text{ cm}^2 \text{s}^{-1}$ , while the ordinary PP separator had a lower conduction rate of only  $1.0210^{-17} \text{ cm}^2 \text{s}^{-1}$ .

$\text{cm}^2 \text{s}^{-1}$  (Fig. 3c). This suggests that the new CuMOF-ANFs separator outperforms the traditional polymer separator in terms of lithium ion conduction. Overall, these results indicate that the CuMOF-ANFs separator prepared in this study can effectively meet the requirements of a lithium metal anode battery separator [31,39,40].

The cyclic voltammetry (CV) curves obtained at different scanning rates (Fig. 4a) exhibit two oxidation peaks around  $1.0\text{V}-2 \text{ V}$  and reduction peaks near  $0.6 \text{ V}$  and  $1.75 \text{ V}$ , indicating the electrochemical reaction of Cu-MOF. The presence of a reoxidation peak suggests that the CuMOF-ANFs composite membrane possesses good electrochemical activity, which facilitates the formation of a uniform and stable SEI layer during the process of lithium deposition and dissolution. To evaluate the rate performance of the Li-Li symmetrical battery, the battery was cycled at various current densities including  $0.2\text{C}$ ,  $0.5\text{C}$ ,  $1\text{C}$ ,  $2\text{C}$ , and  $5\text{C}$ . The corresponding voltage-time profiles are illustrated in Fig. 4b. It can be observed that the battery with the CuMOF-ANFs separator exhibits more stable voltage fluctuations compared to the ordinary battery at different current densities. This indicates that the CuMOF-ANFs separator contributes to enhancing the cycle stability of the battery. As the Fig. 4c shown, the cycle performance of the CuMOF-ANFs composite separator was evaluated by conducting 110 cycles at a temperature of  $25^\circ\text{C}$ , using a fixed charge-discharge current density of  $1 \text{ mA/cm}^2$ . Fig. 4c illustrates the results, showing that after 110 cycles, the battery discharge capacity retention rate of the CuMOF-ANFs separator was approximately 96 %. This retention rate was significantly higher than that of the battery assembled with an ordinary separator, which only retained about 75 % of its discharge capacity. These findings indicate that the CuMOF-ANFs composite separator exhibits excellent cycle stability for lithium metal anode batteries. Furthermore, it was observed that the CuMOF-ANFs system achieved nearly 100 % coulomb efficiency after 110 cycles. This observation further supports the notion that the good stability of the battery is attributed to the presence of the aramid nanofiber and

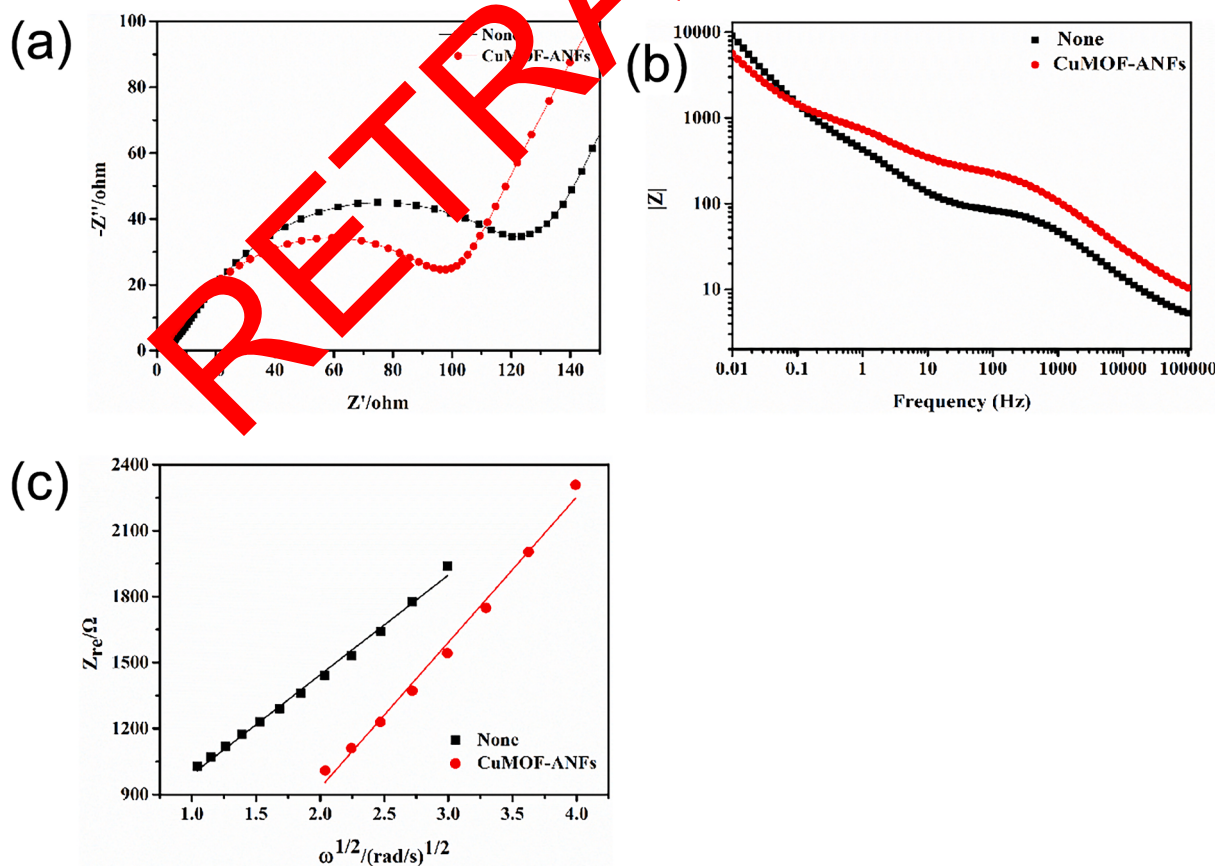
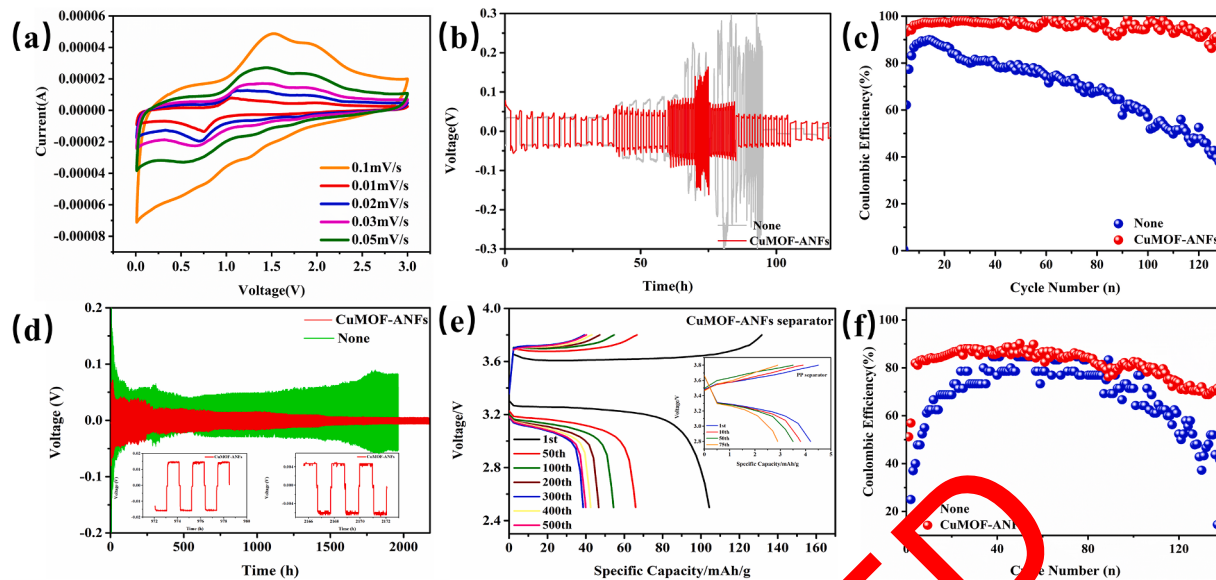


Fig. 3. (a) EIS profiles of the cell using the CuMOF-ANFs separator (b) Bode plots of CuMOF-ANFs separator (c) Linear diagram of angular frequency and impedance.



**Fig. 4.** (a) Cyclic voltammetry (CV) scans of the Li-Cu half-cell (b) Rate performance of Li-Li battery (c) Coulombic efficiency of Li plating test with CuMOF-ANFs separator cells (red) and normal cells (blue) at current densities of  $1 \text{ mA/cm}^2$  ( $1 \text{ mAh/cm}^2$ ) (d) Cycling performance of the Li|Li cells with different separators at a current density of  $1 \text{ mA/cm}^2$  (e) Voltage profiles of CuMOF-ANFs separator and PP separator (f) Coulombic efficiency of Li plating test with CuMOF-ANFs separator cells (red) and normal cells (blue) at current densities of  $1 \text{ mA/cm}^2$  ( $1 \text{ mAh/cm}^2$ ).

CuMOF structure. These components provide a 3D porous mesh structure for the CuMOF-ANFs separator, enhancing its Young's modulus. This improvement in mechanical properties is beneficial for inhibiting the growth of lithium dendrites and preventing short circuits during the long-term cycling process. Overall, these results demonstrate the potential of CuMOF-ANFs composite separators in enhancing the performance and safety of lithium metal batteries [19]. During the test period with a current density of  $1 \text{ mA/cm}^2$ , the voltage distribution of the lithium-ion symmetric battery coated with the CuMOF-ANFs composite separator remained relatively stable for a duration of 2000 h (Fig. 4d). As shown in figure S4, the voltage fluctuation amplitude of the battery with CuMOF-ANFs separator is stable at about 900 and 1200 h of cycling. This indicates that the composite coating on the separator effectively mitigates fluctuations in voltage and reduces the lithium stripping/plating potential. The voltage distribution of the Li-Li symmetric cells without coated separator, on the other hand, showed large and irregular fluctuations, indicating poor cyclic stability. Furthermore, the lithium stripping/plating potential in the Li-Li symmetric cells with the CuMOF-ANFs composite coated separator was consistently low ( $< 20 \text{ mV}$ ), indicating a more stable electrode performance. In contrast, the Li-Li symmetric cells without coated separators exhibited a high lithium stripping/plating potential, indicating a less stable electrode performance. These results demonstrate that the CuMOF-ANFs composite coated separator significantly improves the cyclic stability and electrode performance of Li-Li symmetric cells. The presence of the composite coating on the separator helps to maintain a stable voltage distribution and reduce the lithium stripping/plating potential, resulting in enhanced cyclic stability and performance. In conclusion, the CuMOF-ANFs composite coated separator is a promising solution for improving the performance and stability of Li-Li symmetric cells. It effectively addresses the challenges associated with voltage fluctuations and lithium stripping/plating potential, thereby enhancing the overall performance and safety of lithium metal batteries [30]. In order to further test the catalytic effect of the CuMOF-ANFs separator on the electrochemical performance of the lithium metal anode battery, the performance of the CuMOF-ANFs separator in the full cells will be studied. The polarization voltage of the full cells with the CuMOF-ANFs-coated separator stabilized at about 0.54 V after 500 cycles at a current density of  $1 \text{ mA/cm}^2$  for the whole battery (as shown in

**Fig. 4e**) In contrast, the voltage of the battery utilizing the PP separator was less stable and could not complete the full 500 cycles as expected (as shown in figure S5) [36]. The Coulombic efficiency was employed as a robust validation method to further evaluate the electrochemical stability of the full battery. Based on the Fig. 4f, it can be inferred that the inclusion of CuMOF-ANFs separators in a full battery significantly enhances its Coulombic efficiency and stability compared to batteries with conventional dividers, particularly after 140 cycles. The Coulombic efficiency of a full battery with a PP separator rapidly decreases, whereas conversely, a full battery equipped with a CuMOF separator can achieve approximately 80 % efficiency. This observation underscores the potential of CuMOF-ANFs separators in enhancing the overall electrochemical performance of batteries. This excellent performance results show that CuMOF-ANFs separator can not only inhibit the growth of lithium dendrites, but also significantly improve the deposition of lithium metal and improve the electrochemical performance of lithium metal anode batteries. This excellent performance further demonstrates the potential of this new 3D porous mesh separator in practical applications.

#### 4. Conclusion

The novel CuMOF-ANFs composite separator with a three-dimensional porous mesh structure was investigated in this study. The separator possesses high ionic conductivity, and stable electrochemical activity. By incorporating aramid cellulose into CuMOF, the composite separator demonstrates significantly improved electrochemical performance compared to traditional separators. The CuMOF-ANFs composite separator effectively inhibits the growth of lithium dendrites, facilitates efficient charge transfer at the separator-electrode interface, and forms a uniform and stable solid electrolyte interphase (SEI) layer during lithium deposition and dissolution. As a result, the cyclic stability and cycle life of lithium metal anode batteries are greatly enhanced. The experimental results reveal that the 24.855 nm CuMOF-ANFs separator achieves a Coulomb efficiency of 96 % after 110 cycles at a current density of  $1 \text{ mAh/cm}^2$ . Furthermore, the long-cycle test demonstrates stable voltage fluctuation even after 2000 h under the same conditions. Finally, full batteries with a CuMOF-ANFs separator can still maintain a stable voltage of around 0.54 V after 500 cycles. In addition, the

preparation process of this new type of separator is relatively simple and can be large-scale production. In general, the prepared three-dimensional porous mesh structure of CuMOF-ANFs separator provides a new way to solve the problem of short circuit during the cycle of lithium metal anode battery, the excellent performance of the CuMOF-ANFs separator is also conducive to lithium metal to overcome the shortcomings of lithium dendrites, is expected to replace graphite as the next generation of high-capacity, high-current density battery potential.

### CRediT authorship contribution statement

**Manshu Zhang:** Conceptualization, Formal analysis, Validation, Methodology, Writing – original draft. **Liming Wu:** Validation, Data curation, Writing – original draft. **Tao Yang:** Conceptualization, Writing – review & editing, Methodology, Supervision. **Bing Zhu:** Data curation, Validation, Visualization. **Yangai Liu:** Writing – review & editing, Funding acquisition.

### Declaration of competing interest

The authors declare that they have no known competing financial interests or personal relationships that could have appeared to influence the work reported in this paper.

### Data availability

Data will be made available on request.

### Acknowledgement

This work was supported by “the National Natural Science Foundation of China” (Grant No. U22A20130).

### Supplementary materials

Supplementary material associated with this article can be found, in the online version, at [doi:10.1016/j.surfin.2024.104081](https://doi.org/10.1016/j.surfin.2024.104081).

### References

- [1] E.C. Evans, Lithium batteries: to the limits of lithium, *Nat. Int. Wkly. J. Sci.* (2015).
- [2] M.D. Tikekar, S. Choudhury, Z. Tu, L.A. Archer, Design principles for electrolytes and interfaces for stable lithium-metal batteries, *Nat. Energy* 1 (2016) 16114.
- [3] L. Fan, H.L. Zhuang, W. Zhang, Y. Li, Z. Liang, Y. Lu, Facile lithium electrodeposition at ultra-high current densities induced by 3D PMF/Li composite anode, *Adv. Energy Mater.* 8 (2018).
- [4] Q. Li, F.-L. Zeng, Y.-P. Guan, Z.-Q. Lin, Y. Wang, X. Zhang, M. Yao, W.-K. Wang, A.-B. Wang, Poly(dimethylsiloxane)-modified lithium anode for enhanced performance of lithium-sulfur batteries, *Energy Storage Mater.* 13 (2018) 151–159.
- [5] P. Zou, Y. Wang, S.W. Chiang, X. Wei, F. Kang, C. Yang, Directing lateral growth of lithium dendrites in micro-compartmentalized anode arrays for safe lithium metal batteries, *Nat. Commun.* 9 (2018) 464.
- [6] C.Z. Zhao, X.Q. Zhang, X.B. Cheng, R. Zhang, R. Xu, P.Y. Chen, H.J. Peng, J. Q. Huang, Q. Zhang, An anion-immobilized composite electrolyte for dendrite-free lithium metal anodes, *Proc. Natl. Acad. Sci. U.S.A.* 114 (2017) 11069–11074.
- [7] Y. Ma, Z. Zhou, C. Li, L. Wang, Y. Wang, X. Cheng, P. Zuo, C. Du, H. Huo, Y. Gao, G. Yin, Enabling reliable lithium metal batteries by a bifunctional anionic electrolyte additive, *Energy Storage Mater.* 11 (2018) 197–204.
- [8] X. Wang, W. Zeng, L. Hong, W. Xu, H. Yang, F. Wang, H. Duan, M. Tang, H. Jiang, Stress-driven lithium dendrite growth mechanism and dendrite mitigation by electroplating on soft substrates, *Nat. Energy* 3 (2018) 227–235.
- [9] K.-H. Chen, K.N. Wood, E. Kazyak, W.S. LePage, A.L. Davis, A.J. Sanchez, N. P. Dasgupta, Dead lithium: mass transport effects on voltage, capacity, and failure of lithium metal anodes, *J. Mater. Chem. A* 5 (2017) 11671–11681.
- [10] S. Liu, X. Xia, Y. Zhong, S. Deng, Z. Yao, L. Zhang, X.B. Cheng, X. Wang, Q. Zhang, J. Tu, 3D TiC/C Core/Shell nanowire skeleton for dendrite-free and long-life lithium metal anode, *Adv. Energy Mater.* (2018) 1702322.
- [11] X. Judez, H. Zhang, C. Li, G. Eshetu, G.-G. Eshetu, J.A. Gonzalez-Marcos, Review-solid electrolytes for safe and high energy density lithium-sulfur batteries: promises and challenges, *J. Electrochem. Soc.* (2018).
- [12] L. Yayuan, L. Dingchang, L. Yuzhang, C. Guangxu, P. Allen, N. Oliver, L. Yanbin, C. Yi, Solubility-mediated sustained release enabling nitrate additive in carbonate electrolytes for stable lithium metal anode, *Nat. Commun.* 9 (2018), 3656.
- [13] Poly(dimethylsiloxane) thin film as a stable interfacial layer for high-performance lithium-metal battery anodes, *Adv. Mater.* (2017) 29.
- [14] C.B. Bucur, A. Lita, N. Osada, J. Muldoon, A soft, multilayered lithium–electrolyte interface, *Energy Environ. Sci.* (2015).
- [15] C.P. Yang, Y.X. Yin, S.F. Zhang, N.W. Li, Y.G. Guo, Accommodating lithium into 3D current collectors with a submicron skeleton towards long-life lithium metal anodes, *Nat. Commun.* 6 (2015) 8058.
- [16] J. Xiao, P. Zhai, Y. Wei, X. Zhang, Y. Gong, In-situ formed protecting layer from organic/inorganic concrete for dendrite-free lithium metal anodes, *Nano Lett.* (2020).
- [17] I. Vrejoiu, D.J. Pedarnig, M. Dinescu, S. Bauer-Gogonea, D. Bauerle, Flexible ceramic-polymer composite films with temperature-insensitive and tunable dielectric permittivity, *Appl. Phys. A Mater. Sci. Process.* (2002).
- [18] Y.Y. A, C.H. A, G.G. B, C.H. A, L.L. A, J.X. A, Aramid nanofiber/bacterial cellulose composite separators for lithium-ion batteries, *Carbohydr. Polym.* 247 (2020) 116702.
- [19] C. Zhu, J. Zhang, J. Xu, X. Yin, H. Wang, Aramid nanofibers/polyphenylene sulfide nonwoven composite separator fabricated through a facile papermaking method for lithium ion battery, *J. Membr. Sci.* 588 (2019) 117169.
- [20] M. Yanilmaz, Novel nanofiber-based membrane separators for lithium-ion batteries, 2015.
- [21] P. Wu, Y. Wu, K. Zhu, G. Meng, A. Lin, A. Ze, X. Chen, K. Li, Nickel-based metal–organic framework-derived Ni/NC/KO<sub>2</sub> as a separator coating for high capacity lithium-sulfur batteries, *Sustain. Energy Fuels* 5 (2021) 6372–6380.
- [22] B. Dang, Q. Li, Y. Li, Y. R. Zhao, J. Li, F. Wu, Metal-organic framework-based glass fiber separator and its efficacy as polymer electrolyte barrier and dendrite suppressor for lithium-sulfur batteries, *Alloys Compd.* (2022) 915.
- [23] A. Valverde, C. Go, J. A. M., M.M. Sosa, S. Wuttke, R.F.d. Luis, Metal-organic framework-based PVDF separators for high rate cycling lithium-ion batteries, *ACS Appl. Energy Mater.* 3 (2020) 2000.
- [24] H. Guo, L. Li, J. Shen, T. Wang, P. Chen, X. Cong, S. Zhang, H. Jiang, X. Zhao, Controllably regulating ion transport in lithium metal batteries via pore effect of metal-organic framework-based separators, *Appl. Surf. Sci.* 589 (2022), 152885.
- [25] L. Wei, Z. Lihui, F. Kun, Y. Zhi, W. Jiayu, A. Thermally, Conductive separator for stable Li metal anodes, *Nano Lett.* 15 (2015) 6149–6154.
- [26] V. Shrivastav, S. Sundriyal, P. Goel, H. Kaur, S.K. Tuteja, K. Vikrant, K.H. Kim, U. K. Tiwari, A. Deep, Metal-organic frameworks (MOFs) and their composites as separators for lithium battery applications: novel means for alternative energy storage, *Coord. Chem. Rev.* 393 (2019) 48–78.
- [27] Y. Liu, Q. Liu, Y. Hong, Y. Xu, Z. Chen, W. Zhao, Z. Hu, J. Wang, H.B. Wu, Solvent sieving separators implement dual electrolyte for highvoltage lithium-metal batteries, *Nano Res.* 16 (2023) 4901–4907.
- [28] L.Y. Yang, J.H. Cao, B.R. Cai, T. Liang, D.Y. Wu, Electrospun MOF/PAN composite separator with superior electrochemical performances for high energy density lithium batteries, *Electrochim. Acta* 382 (2021) 138346.
- [29] S. Fu, L. Wang, T. Zhao, L. Li, F. Wu, R. Chen, Dendrite-free lithium anodes with a metal organic framework-derived cake-like TiO<sub>2</sub> coating on the separator, *ChemElectroChem* 7 (2020).
- [30] T. Yang, Z. Wang, M. Zhang, R. Liu, B. Deng, X. Xing, Y. Liu, Electrolyte additive maintains high performance for dendrite-free lithium metal anode, *Chin. Chem. Lett.* 31 (2020) 1217–1220.
- [31] L. Yue, Y. Xie, Y. Zheng, W. He, S. Guo, Y. Sun, T. Zhang, S. Liu, Sulfonated bacterial cellulose/polyaniline composite membrane for use as gel polymer electrolyte, *Compos. Sci. Technol.* 145 (2017) 122–131.
- [32] J. Liu, S. Min, F. Wang, Z. Zhang, Biomass-derived three-dimensional porous carbon membrane electrode for high-performance aqueous supercapacitors: an alternative of powdery carbon materials, *J. Power Sources* 466 (2020) 228347.
- [33] Y. Cui, X. Zhao, R. Guo, Improved electrochemical performance of La<sub>0.7</sub>Sr<sub>0.3</sub>MnO<sub>3</sub> and carbon co-coated LiFePO<sub>4</sub> synthesized by freeze-drying process, *Electrochim. Acta* 55 (2010) 922–926.
- [34] X. Du, W. He, X. Zhang, Y. Yue, H. Liu, X. Zhang, D. Min, X. Ge, Y. Du, Enhancing the electrochemical performance of lithium ion batteries using mesoporous Li<sub>3</sub>V<sub>2</sub>(PO<sub>4</sub>)<sub>3</sub>/C microspheres, *J. Mater. Chem. B* 22 (2012) 5960–5969.
- [35] Z. Liang, G. Zheng, C. Liu, N. Liu, W. Li, K. Yan, H. Yao, P.C. Hsu, S. Chu, Y. Cui, Polymer Nanofiber-Guided Uniform Lithium Deposition for Battery Electrode, *Nano Lett.* (2015).
- [36] F. Wu, Z. He, L. Liu, S. Guan, F. Wang, Y. Huang, Hierarchical-structure and high-modulus aramid nanofiber membrane protective layer achieving high-performance lithium metal anode, *Chem. Eng. J.* (2023) 471.
- [37] R. Pan, O. Cheung, Z. Wang, P. Tammela, J. Huo, J. Lindh, K. Edstrom, M. Stromme, L. Nyholm, Mesoporous Cladophora cellulose separators for lithium-ion batteries, *J. Power Sources* 321 (2016) 185–192.
- [38] Y. Yang, C. Huang, G. Gao, C. Hu, L. Luo, J. Xu, Aramid nanofiber/bacterial cellulose composite separators for lithium-ion batteries, *Carbohydr. Polym.* 247 (2020) 116702.
- [39] H. Ding, M. Zhong, Y.J. Kim, P. Pholpabu, A. Balasubramanian, C.M. Hui, H. He, H. Yang, K. Matyjaszewski, C.J. Bettinger, Biologically derived soft conducting hydrogels using heparin-doped polymer networks, *ACS Nano* 8 (2014) 4348.
- [40] L. Poole-Warren, N. Lovell, S. Baek, R. Green, Development of bioactive conducting polymers for neural interfaces, *Expert Rev. Med. Devices* (2010).